AIP | Applied Physics Letters

10 nm gap bowtie plasmonic apertures fabricated by modified lift-off process

I-Chun Huang, Jeffrey Holzgrafe, Russell A. Jensen, Jennifer T. Choy, Moungi G. Bawendi, and Marko Lončar

Citation: Applied Physics Letters **109**, 133105 (2016); doi: 10.1063/1.4963689
View online: http://dx.doi.org/10.1063/1.4963689
View Table of Contents: http://scitation.aip.org/content/aip/journal/apl/109/13?ver=pdfcov
Published by the AIP Publishing

10 nm gap bowtie plasmonic apertures fabricated by modified lift-off process

I-Chun Huang,[1] Jeffrey Holzgrafe,[1] Russell A. Jensen ,[2] Jennifer T. Choy,[1]
Moungi G. Bawendi,[2] and Marko Lončar[1,a)]
[1]*John A. Paulson School of Engineering and Applied Sciences, Harvard University, Cambridge, Massachusetts 02138, USA*
[2]*Department of Chemistry, Massachusetts Institute of Technology, Cambridge, Massachusetts 02139, USA*

(Received 13 June 2016; accepted 10 September 2016; published online 26 September 2016)

Bowtie plasmonic apertures, with gap sizes down to 11 nm and silver film thickness of up to 150 nm (aspect ratio ~14:1), were fabricated on a silicon nitride membrane. Transmission spectra feature the aperture resonances ranging from 470 to 687 nm, with quality factors around 10. The mode area of the smallest gap aperture is estimated to be as small as 0.002 $(\lambda/n)^2$ using numerical modeling. Importantly, our fabrication technique, based on an e-beam lithography and a lift-off process, is scalable which allows fabrication of many devices in parallel over a relatively large area. We believe that the devices demonstrated in this work will find application in studying and engineering light-matter interactions. *Published by AIP Publishing.*
[http://dx.doi.org/10.1063/1.4963689]

Metal nanostructures separated by nanometer-scale gaps can have plasmonic resonances which locally enhance the optical field intensity by several orders of magnitude in sub-diffraction volumes.[1,2] These nano-plasmonic devices have a wide variety of applications in systems that rely on strong optical fields, such as surface-enhanced Raman scattering,[3,4] nanoscale nonlinear optics,[5–7] optical tweezing,[8,9] fluorescence enhancement,[10] and large Purcell enhancement of quantum emitters.[11,12] Plasmonic field enhancement becomes much stronger as the gap size is reduced to nanometer scale. This effect has been demonstrated in various applications: Purcell enhancements larger than 1000 were achieved using silver nanowires or nanocubes on metal films with spacing of 5–15 nm;[11,12] surface-enhanced Raman scattering increases by orders of magnitude when the gap of gold dimers decreases;[4] and optical trapping simulations show that tapered 5-nm gap coaxial apertures could trap 2-nm dielectric particle with reasonable laser powers.[13] Thus, a controllable, high yield method to fabricate plasmonic structures with small critical dimensions is a key enabling technology for the field.

There has been much work done to achieve ultrasmall gaps in metal structures. Currently, sub-10-nm gap plasmonic nanostructures can be fabricated by atomic layer deposition followed by ion milling,[14] angled deposition,[15] self-assembly of nanoparticles,[16] chromium expansion with a second lithography,[17] and template stripping from a silicon substrate.[18,19] Among all plasmonic nanostructures, the bowtie apertures (see Figure 1) are one of the more widely used plasmonic resonator structures, having been applied to optical trapping,[20,21] sub-diffraction optical lithography,[22] and molecular fluorescence enhancement.[23] Focused ion beam (FIB) milling is a technique often used to achieve narrow-gap plasmonic aperture devices. For example, Ga^+-FIB has been used to fabricate coaxial[24] and bowtie[25] apertures with gap sizes down to 30 nm. However, realizing smaller gaps can be challenging due to the finite ion beam size and ion-substrate interaction.[24] Recently, researchers have used milling-based He^+-ion lithography (HIL) to produce apertures with even smaller gap sizes, down to 8 nm in coaxial shapes[24] and 5 nm in dimers.[26–28] HIL provides better spatial resolution and lateral smoothness than Ga^+ based FIB.[24] However, both of these techniques are serial in nature, and fabrication of large arrays of devices is challenging. Electron beam lithography (EBL), followed by lift-off or ion milling, is a more scalable approach, capable of producing high resolution features at much a higher production rate. For example, sub-10 nm features were recently developed on hydrogen silsesquioxane (HSQ) EBL resist.[29–31] Furthermore, metal structures with sub-10 nm features have been demonstrated on silicon[32] and silicon nitride membrane substrates.[33,34] However, the thickness of the metal layer that could be patterned (by lift-off) in these works was limited to ~30 nm,[32] which is not sufficient to support non-zeroth order Fabry-Perot type resonances in bowtie nanoapertures.[35,36] Furthermore, thicker metal films are needed to tune the resonance of these modes.

In this work, we developed a modified EBL lift-off process to fabricate large arrays of bowtie apertures with nanoscale gaps and resonances that can be theoretically tuned by controlling the thickness of the metal layer. Using this approach, we fabricated 150 nm thick silver bowtie apertures with gap sizes down to 11 nm (aspect ratio ~14:1). This is better than what has previously been achieved with coaxial metal aperture using Ga^+-ion based FIB (30 nm gap, aspect ratio ~3:1) and is comparable to the results obtained with the He^+ based FIB (8 nm gap, aspect ratio ~13:1).[24] Importantly, our approach is scalable and allows for realization of many devices in parallel. For example, we show that by varying the geometry of the bowties, resonances can be designed to span wide wavelength range, from 470 to 687 nm on one sample. Quality factors of ~12 were measured.

Figure 1(a) shows the schematic of the designed bowtie aperture in a thin silver film, assuming the sidewall is vertical. The light incident on the aperture having polarization across the gap will be mainly coupled to the fundamental gap mode, which is concentrated inside the gap. Figure 1(b)

a)Electronic mail: loncar@seas.harvard.edu

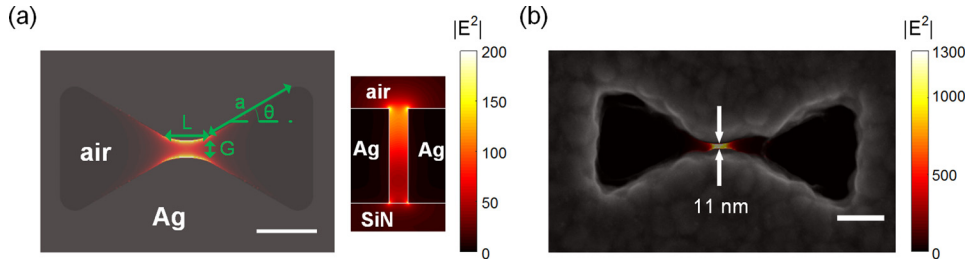

FIG. 1. (a) The schematic and numerical modeling of the designed bowtie and the fundamental gap mode field intensity distribution. The side view field profile shows the Fabry-Perot like resonance with one node inside. G is the gap width, L is the gap length, a is the arm length, and θ is the angle of the arm. Here $L = 82$ nm, $G = 30$ nm, a = 150 nm, and $\theta = 30°$. (b) SEM image of a bowtie aperture with $G = 11$ nm, overlapped with field intensity enhancement profiles at its resonance wavelength. It can be seen that this aperture can have an intensity enhancement as high as 1300. The scale bars are all 100 nm.

shows the mode profile for the 11 nm-gap aperture at its resonance wavelength, obtained using three-dimensional (3-D) finite-difference time-domain (FDTD) simulations (Lumerical), overlaid on the scanning electron microscope (SEM) image of the fabricated structure. The maximum field intensity inside the aperture is found to be ~1300 times stronger than the incident light outside the aperture. Using the definition of energy density in dispersive medium,[37] we also calculate the mode area as small as 0.002 $(\lambda/n)^2$ (normalized to the field at the center of the aperture). We note that the gap mode of bow-tie apertures is always guided no matter how small the gap is (as long as the guided wavelength is below the cutoff, which is defined by the aperture outline), which is not the case in circular apertures.[38] This means that the mode area can be made extremely small and is only limited by the extent to which small gaps to be fabricated. However, a trade-off between mode area and loss due to absorption by the metal needs to be considered.

The fabrication procedure used is outlined in Figure 2(a). Our devices are fabricated on 50 nm thick silicon nitride membranes in order to reduce the resist exposure to back-scattered electrons, and thus improve the resolution of our EBL step. We spin-coated the negative-tone HSQ electron resist (FOX-16, Dow Corning), forming a 0.8 to 1 μm thick resist film on top of the 50 nm silicon nitride membrane with a silicon scaffold (Norcada Inc.). EBL is used (Elionix ELS-F125) to pattern bowtie apertures with the e-beam dosage from 3360 to 4128 μC/cm^2. Then, the sample was developed in tetramethylammonium hydroxide for 17 s, leaving behind tall bowtie posts. The e-beam resist post sidewall is almost vertical, which implies that there is virtually no electron back-scattering from the substrate (left of Figure 2(b)). Next, electron beam evaporation (Denton) was used to evaporate a 2 nm layer of titanium followed by a 150 nm layer of silver. Figure 2(b) shows that silver nanoparticles are deposited on the resist sidewall as well, which complicates the lift-off process. To mitigate this, we used a swab soaked with Isopropanol (IPA) to gently scrub the sample after the evaporation. This step breaks and removes the silver particle-coated posts just above the silver surface. Finally, we submerged the sample in 5:1 BOE (buffered oxide etch) for 130 s to remove the resist inside the aperture. Using this procedure, we could increase the yield of clear bowtie aperture production to almost 100%. We also demonstrated that this method is suitable for realization of bowtie apertures in thicker silver films: for example, we could fabricate 28 nm-gap bowtie apertures in 250 nm thick silver film (supplementary material, Figure S1).

A few heuristics about e-beam writing bowtie posts are also worth mentioning. If the e-beam dosage is too large, the gap size G and aperture itself will increase. However if the dosage is too low, the gap will be closed and the two wings of the bowtie will be disconnected. For the same dosage, G reduces as gap length L increases (due to the proximity effect), and can eventually become zero (the wings get disconnected) if L is too large. Therefore, using the same EBL pattern, the gap size can be tuned by controlling the dosage and gap length. In general, 20-nm gap bowties are easily achievable while the yield of 10-nm gap bowties is lower.

The optical properties of fabricated bowtie apertures were first characterized with a standard optical microscope in transmission mode (Leica DMRX). Light from the halogen lamp is passed through a polarizer to align the polarization across the gap. As seen in the color image in Figure 3(a), different apertures transmit different colors of light in the visible wavelength range. The resonant transmission can

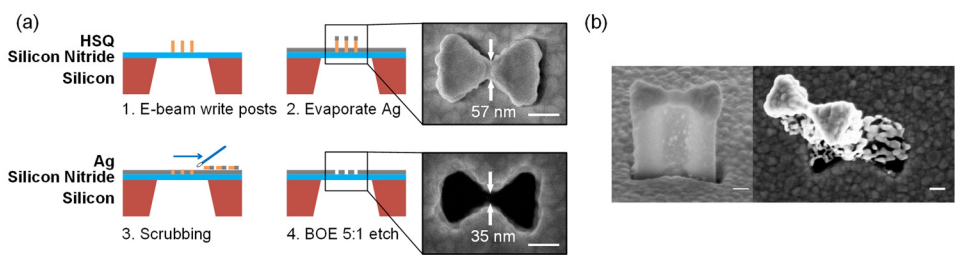

FIG. 2. (a) Schematic of the modified lift-off process used to fabricate our devices. The two SEM images are the top view of the device in steps 2 and 4. Note that the final gap is smaller than the gap of the metal deposited on top of resist. (b) Left: Side view of the device in step 2. The metal evaporation step results in silver particles being deposited on the sidewall, which can compromise the lift-off process. Right panel shows the particles aggregating around the aperture after the lift-off, thus rendering the aperture unusable. To prevent this scrubbing with IPA soaked swab is used, as shown in (a). The scale bars are all 100 nm.

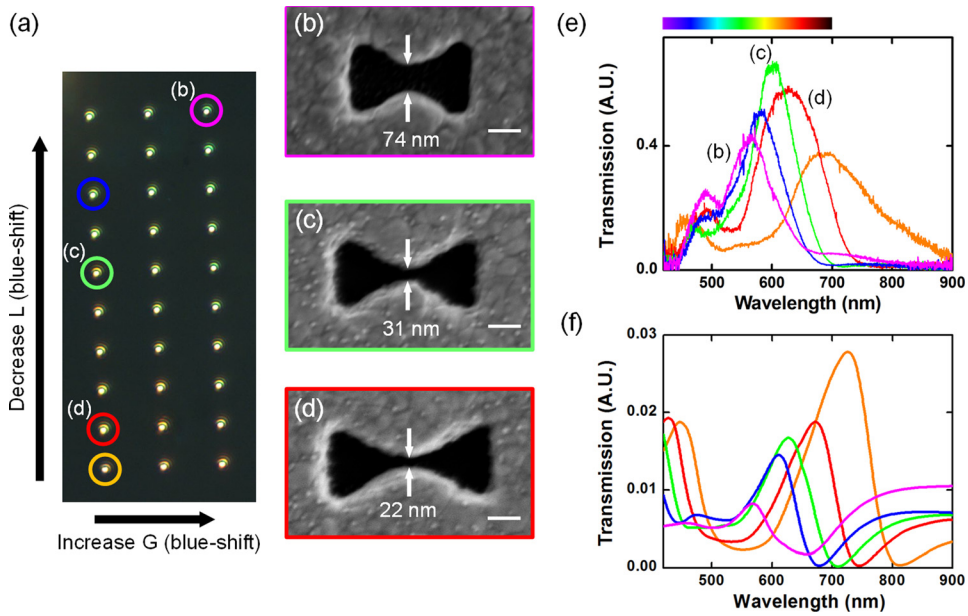

FIG. 3. (a) The transmission optical image of the bowtie array fabricated in 150 nm thick silver layer: gap size G changes with column and gap length L changes with row. Both decreasing L and increasing G will make the resonance blue-shifted. This array shows that the aperture resonance can be tuned smoothly via changing the lateral gap dimensions. Note that the perceived color has a yellow hue due to the yellow halogen lamp light source used in this experiment. (b)–(d) SEM images of three measured bowtie nanoresonators in (a). The SEM image of the orange circled aperture is shown in Fig. 1(b). The e-beam dosage is 3360 μC/cm^2 and the scale bars are all 100 nm. (e) The transmission spectrum of five representative apertures circled in (a), normalized by the emission spectrum of the source. The resonance can be tuned continuously from 565 to 684 nm. (f) The simulated transmission of the five apertures with walls slanted at 20 degrees and rounded top corners with 75 nm radius of curvature in the model. It shows good agreement with the experiments. The colors used in the spectra lines correspond to the circle colors in (a).

be attributed to low-Q Fabry-Perot modes supported by the aperture terminated by air on the one side and silicon nitride membrane on the other side. To quantify these resonances, transmission spectra were measured in a home-built setup (supplementary material, Figure S2) using a spectrometer (Horiba iHR550 with Synapse CCD array). A broadband light source spanning 440–900 nm was generated by a halogen lamp, and a polarizer was used to orient the polarization across the gap. A 0.8 NA objective (~1 μm collection spot size) was used to collect the transmission from individual apertures. This transmitted light was coupled to a fiber which was sent to either an avalanche photodiode (APD) or spectrometer. A piezo stage was used to precisely position the aperture on the collection focal spot as measured by the APD. Transmission data were normalized to the spectrum obtained with the sample removed. The 150 nm thick silver film transmits >25 times less power than the aperture, so we do not expect direct silver transmission to influence the spectra shown below.

The most direct way to tune resonance wavelength is to change the silver film thickness, thus changing the length of the Fabry-Perot-like cavity. However, for a given sample, the film thickness is fixed, so here we demonstrated resonance tuning via control of the lateral gap dimensions of the aperture. The bowtie waveguide mode index (supplementary material, Figure S3) decreases with decreasing L and increasing G, causing resonance blue shift. Figure 3(a) shows the transmission optical microscope image of a bowtie array in which we sweep G and L. In horizontal direction, from left to right, we increased the gap size G. In vertical direction, from bottom to top, we decreased the gap length L, which due to the nature of EBL also increases the gap size (Figures 1(b), 3(c) and 3(d)), as discussed above. The used EBL dosage is 3360 μC/cm^2. As shown in the optical image (Figure 3(a)), the aperture color is blue-shifted toward the top-right (small L and large G). This array also demonstrates the high yield production capability of our fabrication technique. Figure 3(e) shows the experimental transmission spectra of the apertures circled in (a), and quantitatively demonstrates the resonance tuning from 684 nm to 565 nm. The smallest-gap bowtie we can fabricate is 11 nm. We also simulated the transmission spectra of these five apertures and the results match well. The detailed simulation method is described in the later paragraph. Also, see supplementary material for more experimental examples of showing gradual resonance tuning in aperture array (Figure S4).

To further increase the resonance tuning range, we also fabricated the bowtie devices with a smaller outline. The smaller outline will tune the resonance towards shorter wavelength, without increasing the gap and thus sacrificing the enhancement. Figures 4(a)–4(c) show the scanning electron microscope (SEM) images of three smaller bowtie apertures along with their color recorded with the transmission microscope. The measured transmission spectra show resonances at 470, 539, and 605 nm for the three apertures, which match the blue, cyan, and orange colors, respectively, measured using the transmission microscope. Note that Figures 4(b) and 3(b) have similar resonance wavelengths, but Fig. 4(b) has a smaller gap and thus higher field enhancement due to smaller outline design. Despite the rough granular boundaries of the apertures, the resonances show quality factors larger than 6. The smallest aperture has the highest quality factor of all the measured devices at 11.8. However, it is also the dimmest among the three due to the smallest overall size.

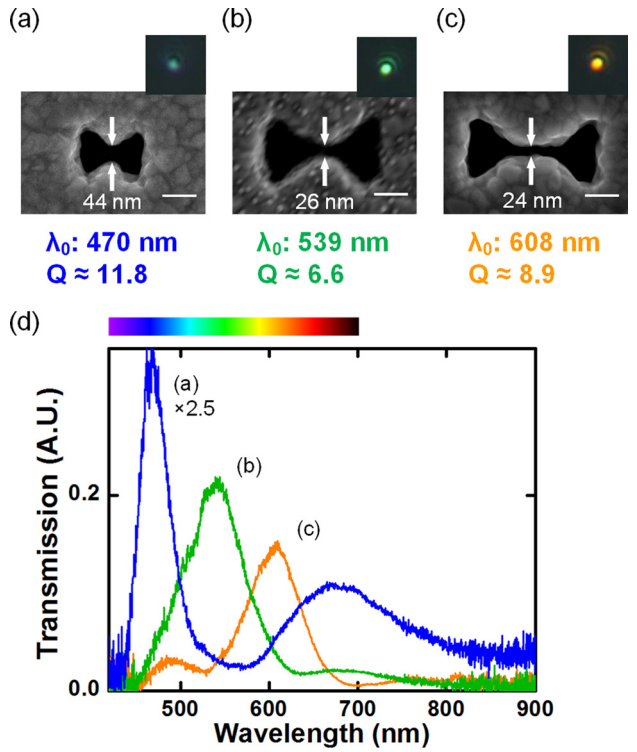

FIG. 4. Resonances can be tuned further blue-shifted by shrinking the overall bowtie outline. (a)–(c) The SEM images of the three measured bowtie nanoresonators. On top right of each image is the optical image under the transmission optical microscope, showing the color of blue, cyan, and orange. The silver thickness is 150 nm, and the scale bars are all 100 nm. (d) The measured transmission spectra of the three apertures, normalized by the emission spectrum of the source. They correspond to the optical images well. The blue resonance has the highest Q factor, which is 11.8.

The measured Q factors are typically 6–8, and are near an order of magnitude smaller than the theoretically predicted material Q of 40–60 in this wavelength range.[39] This suggests our devices' Q factors are mainly limited by the sidewall tapering, surface imperfection, and the radiation loss at the aperture interfaces. From the above SEM images, we can see that the bowtie shape is well-defined by the modified lift-off after e-beam writing posts. However, from the supplementary material Figure S5, it is clear that the boundary of the aperture is mainly defined by large grains, and the surface is not smooth, which is likely a main contributor to the low Q factors. In addition, the sidewall of the aperture is slightly angled since during the evaporation step the silver layer deposited on top of the resist post grows laterally and creates an umbrella effect which blocks the silver depositing on the SiN substrate. We performed SEM imaging at a tilted angle, which showed the wall is slanted by 20°–28° for several apertures (supplementary material, Figure S6). This issue could be solved by performing silver deposition on a tilted and rotating stage. More vertical sidewalls would likely improve the quality factors by creating a more consistent mode propagating through the aperture. The more vertical sidewalls give more abrupt changes at the interfaces, leading to higher reflections and thus higher Q.

We also simulated the transmission spectra of our apertures using a 3-D FDTD algorithm (Lumerical Solutions, Inc.). The aperture geometry was characterized using scanning electron microscope, and SEM images were imported into the simulation program, assuming the sidewalls are vertical. Dielectric properties of the silver film were directly measured via ellipsometry (J.A. Woollam). The simulation peak transmission wavelengths differ quantitatively from experimental results but reproduce the qualitative trend seen in the data: decreasing L or increasing G leads to blue. With the vertical cross section field plot, we confirmed the resonance is a Fabry-Perot like resonance with one node inside (left part of Figure S7). We attribute the quantitative inaccuracy to the tapering of our apertures. To investigate this possibility, we used the bowtie model shown in Figure 1(a) and tapered the sidewall of the bowtie aperture. We assume the sidewalls are slanted by 20° and the top corners are rounded in order to model the aperture geometry more accurately. After modifying these two factors, we can see the simulations match experiments better, suggesting these factors contribute to the remaining discrepancy (Figure 3(f), and right part of Figure S7).

In summary, using EBL and modified lift-off we have fabricated small-gap bowtie metal apertures, with gap dimensions as small as ~11 nm, which have previously been fabricated using more time consuming FIB milling processes. The ability to do large-scale fabrication enables high throughput cavity design optimization and experimentation. Transmission spectra confirm the resonators' resonances and demonstrate Q factors as high as 11.8. The bowtie apertures presented here offer an exciting platform for applications in light-matter interaction engineering, optical tweezing, and surface-enhanced Raman scattering. Thus, they may have applications in coupling to quantum emitters like defect centers in diamond[40] or quantum dots.[41] The use of these apertures to trap and pump colloidal quantum dots with two-photon excitation has already been demonstrated.[21] Finally, with ultrasmall mode area and clear colors, these apertures may find useful as ultrasmall color pixels.[42]

See supplementary material for the figures mentioned in the manuscript: SEM images of bowtie apertures at normal and tilted angle, setup schematic, additional transmission data, and improved simulations done with slanted-rounded rather than vertical sidewalls.

The research described in this paper was supported by the Air Force Office of Scientific Research (AFOSR) Multi-University Research Initiative (MURI) program on Metamaterials (FA9550-14-1-0389), and by the Center for Excitonics, an Energy Frontier Research Center funded by the U.S. Department of Energy, Office of Science, Basic Energy Sciences (BES) under Award No. DE-SC0001088. The devices were fabricated at the Center for Nanoscale Systems at Harvard University. The authors thank Professor Karl Berggren, Shota Kita, and Cheng Wang for guidance and fruitful discussions.

[1]D. K. Gramotnev and S. I. Bozhevolnyi, Nat. Photonics **4**(2), 83–91 (2010).
[2]J. A. Schuller, E. S. Barnard, W. Cai, Y. C. Jun, J. S. White, and M. L. Brongersma, Nat. Mater. **9**(3), 193–204 (2010).
[3]D. K. Lim, K. S. Jeon, H. M. Kim, J. M. Nam, and Y. D. Suh, Nat. Mater. **9**(1), 60–67 (2010).
[4]W. Zhu and K. B. Crozier, Nat. Commun. **5**, 5228 (2014).

[5]S. Kim, J. Jin, Y. J. Kim, I. Y. Park, Y. Kim, and S. W. Kim, Nature **453**(7196), 757–760 (2008).
[6]P. Genevet, J. P. Tetienne, E. Gatzogiannis, R. Blanchard, M. A. Kats, M. O. Scully, and F. Capasso, Nano Lett. **10**(12), 4880–4883 (2010).
[7]M. Kauranen and A. V. Zayats, Nat. Photonics **6**(11), 737–748 (2012).
[8]M. L. Juan, R. Gordon, Y. Pang, F. Eftekhari, and R. Quidant, Nat. Phys. **5**(12), 915–919 (2009).
[9]Y. Pang and R. Gordon, Nano Lett. **11**(9), 3763–3767 (2011).
[10]A. Kinkhabwala, Z. Yu, S. Fan, Y. Avlasevich, K. Müllen, and W. E. Moerner, Nat. Photonics **3**(11), 654–657 (2009).
[11]K. J. Russell, T.-L. Liu, S. Cui, and E. L. Hu, Nat. Photonics **6**(7), 459–462 (2012).
[12]G. M. Akselrod, C. Argyropoulos, T. B. Hoang, C. Ciracì, C. Fang, J. Huang, D. R. Smith, and M. H. Mikkelsen, Nat. Photonics **8**(11), 835–840 (2014).
[13]A. A. Saleh and J. A. Dionne, Nano Lett. **12**(11), 5581–5586 (2012).
[14]H. Im, K. C. Bantz, N. C. Lindquist, C. L. Haynes, and S. H. Oh, Nano Lett. **10**(6), 2231–2336 (2010).
[15]J. Theiss, P. Pavaskar, P. M. Echternach, R. E. Muller, and S. B. Cronin, Nano Lett. **10**(8), 2749–2754 (2010).
[16]J. A. Fan, C. Wu, K. Bao, J. Bao, R. Bardhan, N. J. Halas, V. N. Manoharan, P. Nordlander, G. Shvets, and F. Capasso, Science **328**(5982), 1135–1138 (2010).
[17]W. Zhu, M. G. Banaee, D. Wang, Y. Chu, and K. B. Crozier, Small **7**(13), 1761–1766 (2011).
[18]A. Zehtabi-Oskuie, A. A. Zinck, R. M. Gelfand, and R. Gordon, Nanotechnology **25**(49), 495301 (2014).
[19]X. Chen, C. Ciraci, D. R. Smith, and S. H. Oh, Nano Lett. **15**(1), 107–113 (2015).
[20]J. Berthelot, S. S. Acimovic, M. L. Juan, M. P. Kreuzer, J. Renger, and R. Quidant, Nat. Nanotechnol. **9**(4), 295–299 (2014).
[21]R. A. Jensen, I. C. Huang, O. Chen, J. T. Choy, T. S. Bischof, M. Lončar, and M. G. Bawendi, ACS Photonics **3**(3), 423–427 (2016).
[22]X. Wen, L. M. Traverso, P. Srisungsitthisunti, X. Xu, and E. E. Moon, Appl. Phys. A **117**(1), 307–311 (2014).
[23]G. Lu, W. Li, T. Zhang, S. Yue, J. Liu, L. Hou, Z. Li, and Q. Gong, ACS Nano **6**(2), 1438–1448 (2012).
[24]M. Melli, A. Polyakov, D. Gargas, C. Huynh, L. Scipioni, W. Bao, D. F. Ogletree, P. J. Schuck, S. Cabrini, and A. Weber-Bargioni, Nano Lett. **13**(6), 2687–2691 (2013).
[25]L. Wang, S. M. Uppuluri, E. X. Jin, and X. Xu, Nano Lett. **6**(3), 361–364 (2006).
[26]O. Scholder, K. Jefimovs, I. Shorubalko, C. Hafner, U. Sennhauser, and G. L. Bona, Nanotechnology **24**(39), 395301 (2013).
[27]Y. Wang, M. Abb, S. A. Boden, J. Aizpurua, C. H. de Groot, and O. L. Muskens, Nano Lett. **13**(11), 5647–5653 (2013).
[28]H. Kollmann, X. Piao, M. Esmann, S. F. Becker, D. Hou, C. Huynh, L. O. Kautschor, G. Bosker, H. Vieker, A. Beyer, A. Golzhauser, N. Park, R. Vogelgesang, M. Silies, and C. Lienau, Nano Lett. **14**(8), 4778–4784 (2014).
[29]K. Yamazaki and H. Namatsu, Jpn. J. Appl. Phys., Part 1 **43**(6B), 3767–3771 (2004).
[30]J. K. W. Yang and K. K. Berggren, J. Vac. Sci. Technol., B **25**(6), 2025 (2007).
[31]V. R. Manfrinato, L. Zhang, D. Su, H. Duan, R. G. Hobbs, E. A. Stach, and K. K. Berggren, Nano Lett. **13**(4), 1555–1558 (2013).
[32]H. Duan, H. Hu, K. Kumar, Z. Shen, and J. K. W. Yang, ACS Nano **5**(9), 7593–7600 (2011).
[33]A. L. Koh, D. W. McComb, S. A. Maier, H. Y. Low, and J. K. W. Yang, J. Vac. Sci. Technol., B **28**(6), C6O45 (2010).
[34]H. Duan, A. I. Fernandez-Dominguez, M. Bosman, S. A. Maier, and J. K. Yang, Nano Lett. **12**(3), 1683–1689 (2012).
[35]H. Guo, T. P. Meyrath, T. Zentgraf, N. Liu, L. Fu, H. Schweizer, and H. Giessen, Opt. Express **16**(11), 7756–7766 (2008).
[36]I. A. Ibrahim, M. Mivelle, T. Grosjean, J. T. Allegre, G. W. Burr, and F. I. Baida, Opt. Lett. **35**(14), 2448–2450 (2010).
[37]I. Bulu, T. Babinec, B. Hausmann, J. T. Choy, and M. Loncar, Opt. Express **19**(6), 5268–5276 (2011).
[38]B. Prade and J. Y. Vinet, J. Lightwave Technol. **12**(1), 6–18 (1994).
[39]F. Wang and Y. R. Shen, Phys. Rev. Lett. **97**(20), 206806 (2006).
[40]J. T. Choy, I. Bulu, B. J. M. Hausmann, E. Janitz, I. C. Huang, and M. Lončar, Appl. Phys. Lett. **103**(16), 161101 (2013).
[41]A. V. Akimov, A. Mukherjee, C. L. Yu, D. E. Chang, A. S. Zibrov, P. R. Hemmer, H. Park, and M. D. Lukin, Nature **450**(7168), 402–426 (2007).
[42]K. Kumar, H. Duan, R. S. Hegde, S. C. Koh, J. N. Wei, and J. K. Yang, Nat. Nanotechnol. **7**(9), 557–561 (2012).